Atmospheric Environment 241 (2020) 117842

Contents lists available at ScienceDirect

Atmospheric Environment

journal homepage: http://www.elsevier.com/locate/atmosenv

Sources and transformation of nitrate aerosol in winter 2017–2018 of megacity Beijing: Insights from an alternative approach

Zhongyi Zhang [a,b,1], Hui Guan [c,1], Li Luo [a,b], Nengjian Zheng [a,b], Hongwei Xiao [a,b], Yue Liang [a,b], Huayun Xiao [a,*]

[a] Jiangxi Province Key Laboratory of the Causes and Control of Atmospheric Pollution, East China University of Technology, Nanchang, 330013, China
[b] School of Water Resources and Environmental Engineering, East China University of Technology, Nanchang, 330013, China
[c] The State Key Laboratory of Environmental Geochemistry, Institute of Geochemistry, Chinese Academy of Sciences, Guiyang, 550081, China

HIGHLIGHTS

- Two-endmember linear isotopic mixing model can simulate the $\delta^{18}O$ values of NO_3^- oxidized by O_3.
- OH channel accounted for 48% of the wintertime NO_3^- production in Beijing.
- Vehicular exhaust was the major NO*x* source in winter 2017–2018 of Beijing.

ARTICLE INFO

Keywords:
Nitrate aerosol
$\delta^{15}N$–NO_3^-
$\delta^{18}O$-NO_3^-
Two-endmember isotopic mixing model
Vehicular exhaust

ABSTRACT

The dual isotopic signatures of particulate nitrate (hereafter as $\delta^{15}N$–NO_3^- and $\delta^{18}O$–NO_3^-) have been extensively used to imprint the source and chemical transformation of atmospheric NO*x* (NO*x* = NO + NO_2). For instance, the $\delta^{18}O$–NO_3^- elevated proportionally when NO*x* converted by O_3. In the present study, daily $PM_{2.5}$ samples (n = 91) were collected in winter Beijing (December to February in 2017–2018) and a two-endmember linear isotopic mixing model was used to model the endmember $\delta^{18}O$ values of NO_3^- oxidized by O_3 (termed as $\delta^{18}O_{noct}$) and the contribution of the different pathways (i.e., daytime and nocturnal oxidation pathways). During the campaign, the NO_3^- concentrations in $PM_{2.5}$ varied from 0.3 to 46.3 μg m^{-3} (8.1 ± 9.8 μg m^{-3}), $\delta^{15}N$–NO_3^- from +1.0‰ to +19.6‰ (12.5 ± 3.6‰) and $\delta^{18}O$–NO_3^- from +50.7‰ to +103.5‰ (74.9 ± 13.3‰). The Keeling plots indicated that the $\delta^{18}O_{noct}$ endmember value was within the ranges based on theoretical approaches. The contribution of the nocturnal pathway to NO_3^- in $PM_{2.5}$ ranged from 8.5 ± 3.2% in background days to approximately 100% in extremely polluted days, with a mean of 52.0 ± 25.5%. The determined $\delta^{15}N$–NO_3^- values (12.5 ± 3.6‰) were comparable with previous studies conducted in recent winter Beijing (2013–2017, i.e., average values of 11.9‰–13.8‰). Due to the optimization of energy structure in Beijing, we inferred that the dominant NO*x* source in recent wintertime was the vehicular exhaust. The Bayesian mixing model also confirmed that the contribution of vehicle exhaust/biomass burning sources to the NO_3^- was up to 70%. This study may further improve the understanding of NO*x* emission source and atmospheric processes in urban environments.

1. Introduction

Characterized by extremely high loadings of $PM_{2.5}$ (particulate matters with an aerodynamic diameter less than 2.5 μm), haze pollution episodes have been recorded across China, especially North China Plain (NCP) during the past years (An et al., 2019; Gao et al., 2019; Sun et al., 2016). $PM_{2.5}$ pollution has been noticed as a negative environmental and social problem (An et al., 2019). For example, approximately 1.1million deaths in 2015 in China can be attributed to their long-term exposure to high loadings of $PM_{2.5}$ (Cohen et al., 2017). To alleviate the adverse effects, the Chinese government from central to local has implemented numerous pollution mitigation actions since 2013 (Gao et al., 2019; Zhang et al., 2020a). Taking Beijing as an example, the average annual $PM_{2.5}$ levels in 2017 declined by 35.6% compared with

* Corresponding author.
E-mail address: xiaohuayun@ecut.edu.cn (H. Xiao).
[1] These authors contribute equally.

https://doi.org/10.1016/j.atmosenv.2020.117842
Received 25 March 2020; Received in revised form 26 July 2020; Accepted 3 August 2020
Available online 3 August 2020

that in 2013, from 89 to 58 μg m^{-3} (Li et al., 2019; Zhou et al., 2019). Meanwhile, the gaseous precursors, such as SO_2 and NO*x*, also decreased significantly, while the O_3 increased substantially (Wang et al., 2019a,b; He and Zhang, 2018). Therefore, a better understanding of $PM_{2.5}$ chemistry (e.g., particle properties, sources, and transformation) in the context of pollution control strategies is advantageous for mitigating the air pollution induced by anthropogenic emissions in the future.

The aerosol chemistry of individual species and aerosol properties (e.g., aerosol liquid water content: ALWC and pH) were suggested to change correspondingly with the emission reduction strategies in Beijing since 2013, as demonstrated by field measurements and thermodynamic model simulations (Li et al., 2019; Song et al., 2019a,b; Xu et al., 2019; Zhou et al., 2019). In general, the accumulation of aerosol chemical species significantly affected the particle properties, which in turn influence the production of secondary inorganic and organic species (Gao et al., 2019; Li et al., 2019; Song et al., 2019a,b). For instance, the ALWC and acidity of fine-mode particulate (e.g., PM_1) quantified by the thermodynamic model were suggested to decline gradually from 2013 to 2019 (e.g., pH increased from 4.52 to 4.89; ALWC decreased from 12 to 8.5 μg m^{-3}, Li et al., 2019; Song et al., 2019a,b), which may weaken the NO_3^- formation potential through N_2O_5 hydrolysis pathway (Chen et al., 2018; Zheng et al., 2015). The heterogeneous uptake of N_2O_5 on the bulk aerosol surface was responsible for the rapid accumulation of NO_3^- both in winter and summertime in urban environments of NCP, indicated by previous field measurements (Tian et al., 2019; Wang et al., 2018; Wen et al., 2018; Xie et al., 2019; Yun et al., 2018). Particle properties, especially the pH and ALWC not only influence the formation of SO_4^{2-}, but also the accumulation of NO_3^- and NH_4^+ (Guo et al., 2015, 2018). The partition of NO_3^- and NH_4^+ by the formation of NH_4NO_3 was also facilitated at high RH and low temperature (Li et al., 2018). It has been confirmed that the fine-mode NO_3^- plays an increasingly important role in the $PM_{2.5}$ development, not only during the haze period but also during the clean days (Li et al., 2019; Zhou et al., 2019). By comparing the aerosol chemistry from two years field measurements (2011–2012 and 2017–2018), Zhou et al. (2019) reported a substantial decline of all aerosol species (i.e., organics, SO_4^{2-}, Cl^-), except for NO_3^-, due to the rapid decline of SO_2 and NMVOCs emission from coal combustion relative to NO*x* in Beijing and its surrounding regions. The rapid accumulation of NO_3^- in recent wintertime of Beijing was due to its enhanced production in clean and slightly polluted days (with $PM_1 < 100$ μg m^{-3}), a circumstance that was quite different from other regions in China and worldwide (Shah et al., 2018; Tian et al., 2019; Zhou et al., 2019). For example, the increased NO_3^- fraction in fine-mode particle over the eastern United States was owing to the increment of pH (from 0.39 to 1.70, Shah et al., 2018), while the pH of fine-mode aerosol remained at higher levels (higher than 4.5) in urban Beijing indicating that virtually all the generated HNO_3 was shifted to particle phase (Ding et al., 2019; Liu et al., 2017; Xie et al., 2019). Understanding the emission sources and the following atmospheric oxidation process of NO*x* is, therefore, crucial for further mitigating atmospheric NO_3^- and haze pollution, to some extent in the urban environments of Beijing.

In general, particulate NO_3^- is produced from emitted NO*x* via both daytime and nocturnal pathways (R1-R7, Alexander et al., 2009):

$$NO + O_3 \rightarrow NO_2 + O_2 \quad (R1)$$

$$NO + HO_2/RO_2 \rightarrow NO_2 + OH/RO \quad (R2)$$

$$OH + NO_2 + M \rightarrow HNO_3 + M \quad (R3)$$

$$NO_2 + O_3 \rightarrow NO_3 \quad (R4)$$

$$NO_2 + NO_3 + M \rightarrow N_2O_5 + M \quad (R5)$$

$$N_2O_5 + H_2O \text{ or } Cl^-(aq) \rightarrow (2\text{-}f)\ NO_3^-(aq) + f\ ClNO_2(g) \quad (R6)$$

$$NO3 + HC/DMS \rightarrow HNO_3 + \text{products} \quad (R7)$$

The dual isotopic compositions of NO_3^- (δ15N–NO3- and δ18O–NO3-) have been successfully used to trace the sources and characterize the oxidation pathways of NO*x* worldwide (Fang et al., 2011; Chang et al., 2019; Luo et al., 2019; Song et al., 2019a,b; Walters et al., 2016; Wang et al., 2019a,b; Zhang et al., 2020b). For example, the NO*x* emitted from vehicle exhaust was estimated to account for approximately 29 ± 17% to $PM_{2.5}$ NO3- in winter Beijing of 2014 (Song et al., 2019a,b). In general, the foundation of source appointment using the theoretical approaches was the respective endmember values of $\delta^{18}O$–NO_3^- and nitrogen isotopic fractionation factors (εN) associated with the different oxidation pathways (Chang et al., 2019; Walters and Michalski, 2015; Walters and Michalski, 2016; Zong et al., 2017). However, several drawbacks of the theoretical approaches may lead to considerable bias against the NO*x* source appointment. One of them is the wide ranges of $\delta^{18}O$–NO_3^- endmember values produced through daytime and nocturnal pathways, respectively (Walters and Michalski, 2016; Zong et al., 2017). In fact, δ18O–NO3- signatures are an admixture of oxygen atom sources (e.g., NO_2, N_2O_5, O_3, H_2O, OH) associated with the effects of kinetic and/or equilibrium during the chemical conversation of NO*x* to NO3- photochemically or nocturnally (Michalski et al., 2012; Walters et al., 2016). The $\delta^{18}O$ of N_2O_5 and NO_2 were suggested to range from 90‰ to 122‰, while $\delta^{18}O$ of OH from −60.5‰ to −35‰ ($\alpha_{OH/H2O}$ predicted to be 0.9645 at 300 K), which may deviate from the corresponding *in situ* $\delta^{18}O$ signatures. For instance, the nocturnal $\delta^{18}O$–NO_2 (averaging 56.3 ± 7.1‰, Walters et al., 2018) in summer at a small Midwestern city of USA was significantly lower than the assumed values (90‰–122‰). Such a large discrepancy between the theoretical and *in situ* $\delta^{18}O$ signatures of NO_2 may introduce substantial uncertainty in the estimated relative contribution of different oxidation pathways, and will further affect the source estimation propagational due to the linkage between the overall εN value from NO*x* to NO_3^- with the relative contribution of individual oxidation pathways. In the present study, a two-endmember linear isotope mixing model was used to define the endmember values of $\delta^{18}O$–NO_3^- generated through the nocturnal pathway and predict the contribution of different oxidation channels. The objectives were:1) to assess the proportion of different oxidation pathways using an alternative approach; 2) to assess the source appointment of NO*x* in the wintertime of Beijing preliminary.

2. Materials and method

2.1. Field sampling

The campaign was conducted from 1st December 2017 to 28th February 2018 in urban Beijing (Zhang et al., 2020b). Daily $PM_{2.5}$ samples were collected from ambient air upon a building rooftop located at the Chinese Research Academy of Environmental Science of urban Beijing (CRAES, 40°02′N, 116°25′E, Fig. S1). The location is generally registered as a combined area of the school, office, residential, and shopping malls. The site is approximately 2.2 km north of the fifth Ring Road, 3.6 km west of the Olympic Park, very close to the Metro Line 5 (Song et al., 2019a,b). No major industrial emissions and local sources are present in this site. The meteorological parameters were acquired from the nearest weather monitoring station (Olympic station, approximately 3.6 km away). During the sample campaign, a total of 91 samples (88 daily $PM_{2.5}$ samples, 3 blank samples) were collected on quartz fiber filters with a high-volume sampler (KC-1000) at an average flow rate of 1.05 m^3 min^{-1}. Gas-phase HNO_3 and particle-phase nitrate are likely to be collected simultaneously during our campaign, and therefore are regarded as atmospheric nitrate. The quartz fiber filters were pre-combusted at 450 °C for 4h to remove impurity. The collected samples were immediately stored at −20 °C in the fridge.

2.2. Chemical analysis

Major water-soluble inorganic ions (e.g., NH_4^+, NO_3^-, SO_4^{2-}, Na^+, Cl^-, K^+, Ca^{2+}, and Mg^{2+}) in $PM_{2.5}$ filters were extracted using 50 mL

ultrapure water (Millipore, 18.2MΩ) facilitated by the ultrasonic bath at room temperature (Zhang et al., 2020a). The water-soluble ions were determined by Dionex Aquion Ion Chromatography (Thermo Fisher Scientific Inc., Massachusetts, USA). In general, the detection limits were better than 6.5 μg/L (Zhang et al., 2020a).

Determination of dual isotopic compositions of NO_3^- were processed using the bacterial denitrifier method (Casciotti et al., 2002; Sigman et al., 2001; Fang et al., 2015). In general, the denitrifying bacteria (*Pseudomonas aureofaciens*, ATCC 13985#) can quantitatively convert the extracted NO_3^- into gaseous N_2O due to the lack of N_2O reductase enzyme. N_2O was then concentrated and delivered into a GasBench-II coupled with a continuous flow isotope ratio mass spectrometer (IRMS; Thermo Fisher Delta V Advantage, Thermo Fisher Scientific, Inc.) for isotopic determination. International nitrate isotopic standards with certified values (USGS32, USGS34, USGS35, and IAEA-N3) were used for data calibration. The presence of NO_2^- has minor influence on the dual isotopic signatures of NO_3^-, since the ratio of NO_2^- to NO_3^- was generally less than 2% during the campaign. N and O isotopic values were reported with the standard delta notation (δ, ‰) in relative to N_2 in air and VSMOW, respectively:

$$\delta^{15}N\text{–}NO_3^- = [(^{15}N/^{14}N)_{sample}/(^{15}N/^{14}N)_{N2\ in\ air} - 1] \times 1000$$

$$\delta^{18}O\text{–}NO_3^- = [(^{18}O/^{16}O)_{sample}/(^{18}O/^{16}O)_{VSMOW} - 1] \times 1000$$

The standard deviations for $\delta^{15}N\text{–}NO_3^-$ and $\delta^{18}O\text{–}NO_3^-$ quantified by 20 replicates of standards were usually better than ±0.2‰ and ±0.8‰, respectively (Zhang et al., 2020b). The reported $\delta^{15}N\text{–}NO_3^-$ was also corrected for the interference of mass-independent $^{14}N\text{–}^{14}N\text{–}^{17}O$ to the N_2O, since the aerosol NO_3^- was associated with substantial mass-independent ^{17}O anomaly. Given that the measurements of $\delta^{17}O$ were not available in our laboratory at present, published relationships between $\delta^{18}O$ and $\Delta^{17}O$ were used in this study.

2.3. Thermodynamic model for pH and ALWC simulations

The particle phase of NO_3^- keeps in chemical equilibrium with the gas-phase HNO_3, which is controlled primarily by particle acidity. ISORROPIA-II model (website: http://isorropia.eas.gatech.edu/, last access: 21 February 2020) was used to simulate particle properties (i.e., ALWC, pH) and the gas-particle partitioning of semi-volatile species (Fountoukis and Nenes, 2007; Guo et al., 2015). The primary assumption of running the ISORROPIA-II model was that the particle was mixed internally with no solid precipitates when relative humidity>30%. Usually, the ISORROPIA-II model was run in "forward mode" and assumed a metastable state of aerosol, since the forward mode was suggested insensitivity to the measurement errors (Fountoukis and Nenes, 2007). Moreover, forward mode demanded the input of total concentrations of semi-volatile species (gas + particle phase, e.g., NH_3+NH_4^+) for better predictions. However, concurrent measurements of gas and particle-phase concentrations were unavailable. To this end, the ISORROPIA-II model was run iteratively until the output NO_3^- and NH_4^+ within <1% by mass with the determined particle concentrations for ALWC and pH simulation. The model was performed with RH>30% in the present study.

2.4. Prediction of $\delta^{18}O\text{–}NO_3^-$ endmember values and specific-pathway contribution

The previous theoretical approaches using $\delta^{18}O\text{–}NO_3^-$ to predict the contribution of specific-pathway usually presumed that the $\delta^{18}O$ of O-bearing molecules related to NO*x* oxidation varied in relatively wide ranges to embrace the variety of atmospheric circumstances, e.g., $\delta^{18}O\text{–}H_2O$ ranged from −25‰ to 0‰, $\delta^{18}O\text{–}OH$ from −60.5‰ to −35‰; $\delta^{18}O\text{–}N_2O_5$ and $\delta^{18}O\text{–}NO_2$ from 90‰ to 122‰ (Zong et al., 2017). It should be noted that the broad ranges of $\delta^{18}O\text{–}N_2O_5$ or $\delta^{18}O\text{–}NO_2$ were even equivalent to half of the seasonal variations of *in situ* $\delta^{18}O\text{–}NO_3^-$ (e.g., from 49.4‰ to 103.9‰ at an environmental monitoring station of the State Ocean Administration of China, Zong et al., 2017). This implied considerable uncertainty in the estimation of proportional contribution of specific-pathway by the theoretical approaches. In the present study, we proposed an alternative approach to resolve the respective contributions of the two-generation pathways as follows.

2.4.1. Endmember of $\delta^{18}O\text{–}NO_3^-$ produced via OH oxidation pathway

Based on comprehensive field measurements, Wang et al. (2017a,b) documented that the contribution of nocturnal pathways (e.g., N_2O_5 hydrolysis and NO3+HC channel) to the accumulation of NO_3^- during the clean periods was negligible in Beijing of 2016 (September 11 to October 4), with the level less than 0.1 μg m^{-3} per night because of the low concentrations of the aerosol surface. The magnitude of NO_3^- from the nocturnal channel, therefore, only accounted for one-tenth of the total sink of NO_3^-. Furthermore, isotopic approaches (i.e., $\delta^{18}O\text{–}NO_3^-$ and $\Delta^{17}O\text{–}NO_3^-$) also suggested the dominant role of OH oxidation in nitrate production during clean periods (Zhang et al., 2019; Fig. S5 of Zong et al., 2017). Inspired from these evidences, we suggested that the $\delta^{18}O\text{–}NO_3^-$ of $PM_{2.5}$ in background days (extremely clean days, see 3.1 of Results and Discussion) may be served as a trustworthy substitution of theoretical endmember $\delta^{18}O$ values of product NO_3^- generated from the daytime channel ($\delta^{18}O_{day}$). Accordingly, the endmember of $\delta^{18}O_{day}$ was suggested as 54.8‰±4.3‰ in the present study, which compared well with that based on theoretical approaches by assuming 2/3 oxygen atom from NO_2 and 1/3 from OH (i.e., ~55‰ in Fang et al., 2011 and Zong et al., 2017).

2.4.2. Endmember of $\delta^{18}O\text{–}NO_3^-$ produced via nocturnal channels

The linear mixing model, such as the Keeling plot has been frequently used to interpret fluctuations in the isotopic values of ambient atmospheric gas contaminates (e.g., CO_2, CH_4) and to estimate the source signatures being added to the gas pollute under certain conditions (Pataki et al., 2003). The Keeling model can also be used to describe the atmospheric nitrate concentrations and their oxygen isotopic signatures. In general, the majority of $PM_{2.5}$ NO_3^- in the atmosphere is a complete mixture generated via daytime and nocturnal pathways with different proportion (as $\delta^{18}O_{day}$ and $\delta^{18}O_{noct}$ endmember, respectively), confirmed by model simulations and isotopic estimation (Wang et al., 2017a,b, 2018; Yun et al., 2018; Zong et al., 2017; He et al., 2018). Furthermore, the fast-heterogeneous hydrolysis of N_2O_5 associated with ^{18}O-enriched NO_3^- was responsible for the rapid accumulation of NO_3^- in haze periods (Wang et al., 2017a,b; Yun et al., 2018). Since the two endmembers associated with distinct $\delta^{18}O$ isotopic signatures were usually mixed conservatively, the Keeling plot of $\delta^{18}O\text{–}NO_3^-$ against $1/[NO_3^-]$ will be linear and the intercept of Eqn. (1) would correspond to the $\delta^{18}O$ signature of the nocturnal pathway (Phillips and Gregg, 2001):

$$\delta^{18}O\text{–}NO_3^- = a*[1/NO_3^-] + b \quad (1)$$

with the intercept of "b" (when $1/NO_3^- = 0$, implying extremely nitrate aerosol pollution) representing the endmember values of $\delta^{18}O_{noct}$. The contribution of the nocturnal channel to daily NO_3^- in $PM_{2.5}$ (termed as f_{noct}) can be estimated using Eq (2):

$$f_{noct} = [\delta^{18}O\text{–}NO_3^- - \delta^{18}O_{day}]/[\ \delta^{18}O_{noct} - \delta^{18}O_{day}] \quad (2)$$

The overall potential uncertainty of f_{N2O5} can be estimated by taking the propagation of uncertainty on each factor in Eq. (2) as follows (and Text S1):

$$\sigma^2_{f_{noct}} = \frac{1}{(b-a)^2}\left[\sigma^2_{mix} + f_a^2\sigma_a^2 + f_b^2\sigma_b^2\right] \quad (3)$$

with the mix, b, and a representing $\delta^{18}O\text{–}NO_3^-$, $\delta^{18}O_{noct,}$ and $\delta^{18}O_{day}$, respectively. Detailed information on the Keeling plots and uncertainty analysis was provided in Text S1.

2.5. Source contribution using Bayesian mixing model

NO*x* emitted from coal usage by the end of 2017 reduced significantly due to the stringent control of coal combustion and the optimization of the energy structure (e.g., replace coal with natural gas and electricity, Chang and Ma, 2016). In 2017, coal only accounted for 5.6% of total primary energy consumption in Beijing, while natural gas accounted for 31.8% (Zhang et al., 2020b). Therefore, in our case, four dominant NO*x* emission sources with distinct $\delta^{15}N$ signatures were assigned for the source appointment using Bayesian mixing model of SIMMr: natural gas (−16.5 ± 1.7‰), vehicle exhaust (−3.7 ± 10.4‰), biomass burning (+1.04 ± 4.13‰) and the microbial N cycle (−33.77 ± 12.16‰) (Elliott et al., 2019; Felix and Elliott, 2014; Felix et al., 2012; Walters et al., 2015a,b; Zong et al., 2017). Although the model output all feasible solutions of proportional source contributions, the value of mean ± sd was used in the present study. Since the NO3+HC channel cannot be distinguished based on the $\delta^{18}O$–NO_3^- approach, a previous study conducted in an island located at the Bohai Sea suggested that the total nitrogen isotopic effect of OH and N_2O_5 pathways after multiplying 0.52 was the best solution to simulate the overall εN value from NO*x* to NO_3^-. Clearly, the factor of 0.52 was used to incorporate the NO3+HC channel in the NOx oxidation chemistry. However, we suggested that the approach of multiplying 0.52 cannot be applied directly in the inland city of Beijing, since the proportional contribution of NO3+HC channel in Beijing may differ with that in an island. The nitrogen isotopic fractionation factor of NO*x* converted into NO_3^- used in the present study (εN = 15.6‰±7.4‰) was cited from Song et al. (2020), which conducted in winter 2015 of Beijing (CRAES) and using $\Delta^{17}O$–NO_3^- to estimate the εN values. Detailed information on the practicality of εN was included in Text S2.

3. Results and discussion

3.1. Overview of the wintertime fine aerosol characteristics

Fig. 1 depicted the evolution of aerosol chemical species, meteorological conditions, and other associated aerosol properties (i.e., ALWC, pH) in winter 2017–2018 of urban Beijing. Generally, all the inorganic species showed large variations from the clean to haze episodes. For instance, the NO_3^- concentrations varied from 0.3 to 46.3 μg m^{-3} (8.1 ± 9.8 μg m^{-3}, mean±1sd), while the range of SO_4^{2-} was from 0.5 to 24.9 μg m^{-3} with the mean of 5.2 μg m^{-3}. A relatively high level of Cl^- (2.7 ± 2.1 μg m^{-3}, from 0.2 to 10.9 μg m^{-3}) was observed, implying the likelihood of $ClNO_2$ formation through pathway R4 since the aquatic Cl^- was regarded as the driving factor that controls the $ClNO_2$ generation on the bulk aerosol surface (Mitroo et al., 2019; Wang et al., 2017b; Wen et al., 2015; Yan et al., 2019). Usually, a high amount of particle Cl^- favors the N_2O_5 conversion to $ClNO_2$ and increases the yields of $ClNO_2$ (Mitroo et al., 2019). In theory, the branching generation of $ClNO_2$ would enhance the $\delta^{18}O$ values of product NO_3^- (See Fig. S2 for the explicit chemical mechanism). Other inorganic species, such as NH_4^+ showed a parallel trend with the NO_3^- and SO_4^{2-}.

The ratio of NO_3^-/SO_4^{2-} varied in a wide range, from 0.27 to 3.20 with a mean value of 1.20 (Fig. S3), which was higher than that of winters from 2013 to 2016 (Xu et al., 2019). Interestingly, high ratios of NO_3^-/SO_4^{2-} were always observed in haze days, while low ratios in clean days. Such high ratios of NO_3^-/SO_4^{2-} and its variation trend further indicated the increasing importance of nitrate in the winter particulate pollution, which has been well-documented across China in recent years (Shi et al., 2019; Tian et al., 2019; Xie et al., 2019; Xu et al., 2019). The increasing role of NO_3^- in aerosol pollution may be attributed to the pollution mitigation strategies, in which the NO*x* was simulated to reduce by 38% while the SO_2 by 80% in Beijing since 2013 (Li et al.,

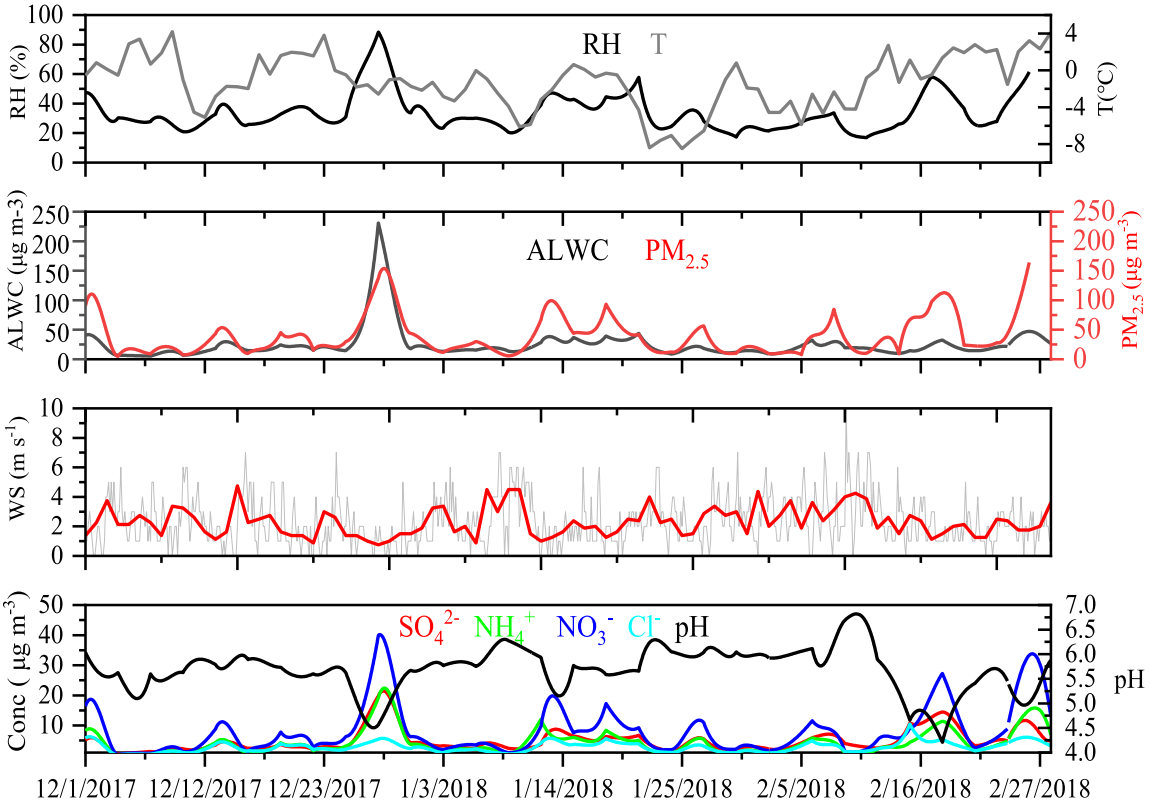

Fig. 1. Time series of several meteorological parameters (i.e.,RH,T,WS: windspeed), mass concentrations of major inorganic species in $PM_{2.5}$ and properties of $PM_{2.5}$ (ALWC: aerosol liquid water content,pH) in winter 2017–2018 of urban Beijing.

2019). Moreover, clean days were usually characterized by lower RH (<30%), while the RH and ALWC significantly increased and aerosol pH remained at a high level (pH > 4.0) when haze occurred (Fig. 1). Such a high pH and ALWC implied that all soluble nitrate preferably partitioned into particle-phase (Fig. S4, "S" curves of nitrate partition), as the equilibrium between gaseous and particle-phase nitrate was predominately controlled by aerosol properties. High ALWC and pH favor the gas-to-particle partition of HNO_3, leading nearly a unit ratio of particle NO_3^- to total soluble nitrate in winter conditions of Beijing (Ding et al., 2019). Another difference between the clean and haze days was the air mass transportation pathways, as presented in Fig. S5. The northern wind with high speed usually leads a lower concentration of gaseous precursors and RH, for example, the clean days NO_2 and CO concentrations were usually less than 20 μg m^{-3} and 0.4 mg m^{-3}, respectively (Fig. 1, Fig. S6). Together, the chemical and meteorological conditions between clean and haze days were distinct. According to the proposal of Tan et al. (2018), the aerosol chemical conditions were classified into three groups (background, clean and polluted days) based on the wind speed and diurnal variation of $PM_{2.5}$ and CO, the proxy for anthropogenic pollution (Fig. S7). Only 10 days were classified as background condition, characterized by an extremely flat level of chemical species and gaseous precursors (e.g., NO_3^-<1 μg m^{-3}), strong northern wind speeds (>4 m/s), low RH (typically<30%) and $PM_{2.5}$ concentrations (<20 μg m^{-3}), which implied the negligible contribution to NO_3^- via N_2O_5 channel (Wang et al., 2018). In the present study, the separation of the clean days from haze episodes was by a threshold value of $PM_{2.5}$ = 40 μg m^{-3}, which corresponding to CO and NO_3^- lower than 1.0 mg m^{-3} and 5 μg m^{-3}, respectively (Fig. S7).

3.2. Dual isotopic signatures of p-NO_3^-

The values of $\delta^{18}O$–NO_3^- in $PM_{2.5}$ have a relatively wide range (74.9 ± 13.3‰), from +50.7‰ to +103.5‰ (Fig. 2), which were within the range of reported values for NO_2 (90–122‰) and H_2O (−20 to 0‰). The measured $\delta^{18}O$–NO_3^- in wintertime $PM_{2.5}$ were also within the range of previous reports conducted in Beijing (e.g., 51.2‰–102.4‰ of winter 2013–2014, Wang et al., 2019a,b). However, the average $\delta^{18}O$–NO_3^- in $PM_{2.5}$ in winter 2017 of Beijing were observed lower than that in January 2015 (88.3 ± 8.5‰, Song et al., 2020), and also smaller than that collected from an island of the Bohai Sea (88.1 ± 10.1‰, Zong et al., 2017), Yongxing Island (83.2‰, Xiao et al., 2015) and Dongshan Island (78.8‰) of southern China sea (Yang et al., 2014). The observed relatively lower $\delta^{18}O$–NO_3^- in $PM_{2.5}$ in 2017–2018 may indicate a significant decline of the heterogeneous generation of NO_3^- through nocturnal pathways, since nocturnal channels were always characterized by ^{18}O-enriched values (Walters and Michalski, 2016). Furthermore, the decline of $\delta^{18}O$–NO_3^- in $PM_{2.5}$ in response to NO*x* emission controls may imply the effectiveness of pollution mitigation strategies, because heterogeneous chemistry was responsible for the rapid explosion of $PM_{2.5}$ during haze periods (Yun et al., 2018; Zheng et al., 2015). Based on online field measurement, frequency of haze episodes with fine PM_1 > 100 μg m^{-3} were observed to decrease substantially in winter from 2011 to 2017 of Beijing, which benefited from the pollution mitigation strategies (Zhou et al., 2019). Also, the ALWC of fine aerosol was modeled to decline in recent winter days (i.e., 12.0 to 8.5 μg m^{-3} of PM_1, Li et al., 2019). Together, these pieces of evidence suggested a reduced N_2O_5 hydrolysis pathway contribution to the NO_3^- accumulation in wintertime.

During the observation period, the $\delta^{15}N$–NO_3^- of $PM_{2.5}$ varied widely from +1.0‰ to +19.6‰, with a mean value of +12.5 ± 3.6‰. In general, the $PM_{2.5}$ $\delta^{15}N$–NO_3^- in 2017 of winter Beijing resembled those sampled in the past few years (e.g., from −2.3‰ to +19.7‰ (+11.9 ± 4.4‰) of winter 2014, Song et al., 2019a,b; −2.5‰ to +19.2‰ (approximately 12.0‰) from December 2014 to January 2015, He et al., 2018; −1.3‰ to +21.2‰ (13.0 ± 4.7‰) from February to April in 2013 at Beijing, Luo et al., 2019). The logical explanation of $\delta^{15}N$–NO_3^- in $PM_{2.5}$ needed a comprehensive understanding of the following effects: $\delta^{15}N$ characteristics of NO*x* emission sources, NO_2 oxidation pathways, isotopic exchange effect associated with the equilibrium between NO and NO_2, kinetic or equilibrium isotopic effect of the oxidation processes and the combination of these effects. To the best of our knowledge, nearly all the coal-fired boilers and plants have been replaced by natural gas in urban Beijing (Zhang et al., 2020b), while the coal combustion for residential heating also switched to natural gas or electricity in rural regions by winter 2017. As the result, the $\delta^{15}N$–NO_3^- in $PM_{2.5}$ of this study should decrease, to some extent when compared with the previous reports (e.g., 2017 *vs* 2013 or 2014), since the NO*x* from coal combustion is typically ^{15}N-enriched while from gas combustion is ^{15}N-depleted (14.5 ± 4.4‰ *vs* −16.5 ± 1.7‰, respectively, Walters et al., 2015a,b). Therefore, source appointment of NO*x* based on the $\delta^{15}N$ signatures of product NO_3^- needed a systematical evaluation of the aforementioned effects, which was tentatively explored in the following discussion.

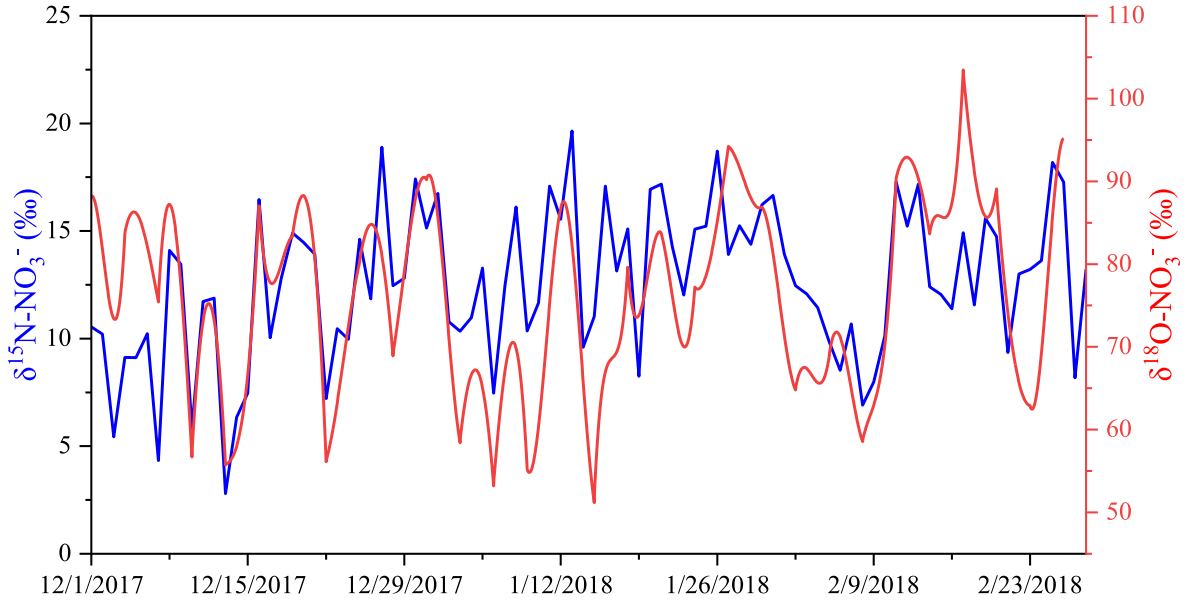

Fig. 2. Time series of $\delta^{15}N$-NO_3^- (blue) and $\delta^{18}O$-NO_3^- (red) in $PM_{2.5}$ collected in Beijing from 12.01.2017 to 02.28.2018. (For interpretation of the references to colour in this figure legend, the reader is referred to the Web version of this article.)

As presented in Fig. 3, the dual isotopic signatures of NO_3^- increased significantly from background days to clean and polluted days, with mean values from 54.8‰ to 65.5‰ and 85.2‰ for $\delta^{18}O$ and 8.5‰–11.9‰ and 14.6‰ for $\delta^{15}N$, respectively. This parallel increasing trend of dual isotopic signatures can be attributed to the enhancement of N_2O_5 hydrolysis pathways from clean to polluted days, in which the product of NO_3^- was associated with enriched ^{15}N and ^{18}O values. Noted that the isotopic equilibrium between NO_2 and N_2O_5 favors the partition of ^{15}N to N_2O_5 ($^{15}\alpha_{N2O5/NO2} = 1.0255$ at 300 K, Walters and Michalski, 2015).

3.3. Endmember $\delta^{18}O$–NO_3^- values and specific-pathways contribution

The intercepts of Keeling plots (Fig. 4) presented that the predicted endmember $\delta^{18}O_{noct}$ value for the whole $PM_{2.5}$ samples was approximately 94.1‰ (±1.4‰). The $\delta^{18}O_{noct}$ value was consistent with that estimated by theoretical approaches (i.e., 93.9 ± 13.2‰). The endmember of $\delta^{18}O_{day}$, represented by that of $\delta^{18}O$–NO_3^- values in background days was suggested as 54.8‰±4.3‰ in the present study. In general, these predicted endmember $\delta^{18}O$–NO_3^- values of both daytime and nocturnal pathways were within the ranges from the theoretical approaches based on numerous assumptions, e.g., $\delta^{18}O$–H_2O ranged from −25‰ to 0‰, $\delta^{18}O$–OH from −60.5‰ to −35‰; $\delta^{18}O$–N_2O_5 and $\delta^{18}O$–NO_2 ranged from 90‰ to 122‰. Therefore, our choice to use $\delta^{18}O$–NO_3^- in background days and intercept of Keeling plots of $\delta^{18}O$–NO_3^- against $1/NO_3^-$ as the atmospheric NO_3^- end-members produced through daytime and nocturnal pathways, respectively, was simple but robust (Text S1).

The uncertainty of the proportional contribution of different oxidation pathways to NO_3^- in $PM_{2.5}$ in daily scale was estimated in the order of 5% by taking into account the propagation of uncertainty on each factor in Eqn. (3) (uncertainties for $\delta^{18}O$–NO_3^-, $\delta^{18}O_{OH}$, and $\delta^{18}O_{noct}$ were 0.8‰, 4.3‰ and 2–3‰, respectively, Text S1), due to the large denominator (e.g., approximately 50‰), which reduced significantly

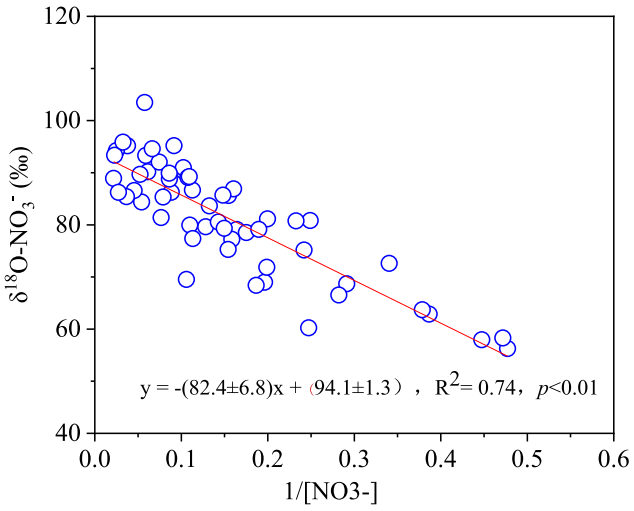

Fig. 4. The measured $\delta^{18}O$-NO_3^- of $PM_{2.5}$ as a function of the parameter [$1/NO_3^-$] (Keeling plots). In theory, the intercept of the regressions represented the endmember values of $\delta^{18}O$-NO_3^- generated via nocturnal pathway.

compared with the theoretical approach (Wang et al., 2019a,b; Zong et al., 2017). The f_{noct} varied widely (mean: 52.0 ± 25.5%), from 8.5 ± 3.2% in background days to approximately 100% in extreme nitrate pollution days (Fig. S8). The large variation of specific-pathway contribution during the campaign can be attributed to the distinct atmospheric chemical conditions (Fig. 1, Fig. S6). In comparison, the contribution of the daytime pathway was approximately 48.0% during the whole period. The fractional contribution of OH oxidation pathways to NO_3^- in winter 2017 was a little higher than that during winter 2014 based on $\Delta^{17}O$–NO_3^- (48 ± 25.5% *vs* 31 ± 11%), which may suggest the

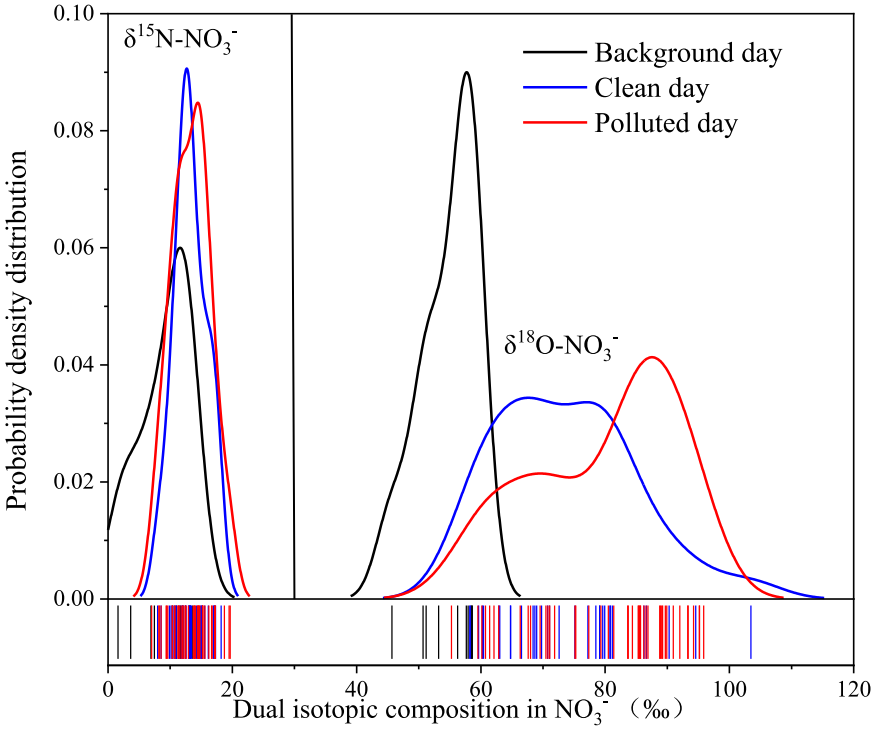

Fig. 3. The distribution density of $\delta^{15}N$-NO_3^- and $\delta^{18}O$-NO_3^- during background (black), clean (blue) and polluted (red) days. The medium of $\delta^{15}N$-NO_3^- and $\delta^{18}O$-NO_3^- shifted positively with the increasing of nitrate aerosol pollution. (For interpretation of the references to colour in this figure legend, the reader is referred to the Web version of this article.)

enhancement of photochemical activity during recent winter seasons. By the direct recording of OH and relevant gaseous species, Lu et al. (2019) observed that the potential of NO*x* oxidation by OH was even 5 times higher than that produced by via N_2O_5 hydrolysis pathways during several haze episodes in winter 2016. Even though, the relative contribution of different oxidation pathways to NO_3^- in $PM_{2.5}$ based on the isotopic approach ($\delta^{18}O$ and $\Delta^{17}O$–NO_3^-) was different with the field measurements (Lu et al., 2019; Wang et al., 2018), which could be explained by the different atmospheric dilution and deposition process between day and night. However, these processes were regarded to exert little influence on the dual isotopic composition of NO_3^- in $PM_{2.5}$.

3.4. Sources contribution to p-NO_3^- using $\delta^{15}N$–NO_3^-

As aforementioned, the ^{15}N isotopic fractionation factors (εN) associated with the following processes: the Leighton cycle (source NO*x*⇌NO_2), kinetic/equilibrium reactions (NO_2→HNO_3), and the source ^{15}N signatures of NO*x* significantly affect the $\delta^{15}N$–NO_3^- values in $PM_{2.5}$. For the effect of the Leighton cycle, the $\delta^{15}N$ of NO_2 and NO_3^- were highly dependent on the mole fraction of NO_2 to the total NO*x* (f_{NO2}), due to the relatively high $\alpha_{NO2/NO}$ values ($\alpha_{NO2/NO} = 1.0356$ at 297K). Usually, $\delta^{15}N$–NO_2 increased with the decreasing of f_{NO2}, e.g., $\delta^{15}N$–NO_2 enriched by 16.3‰ when f_{NO2} decreased from 1 to 0.55 (Walters et al., 2016). The f_{NO2} is generally controlled by the O_3 concentration and NO_2 photolysis rate during the daytime, while f_{NO2} tends to approach 1 at night (Walters et al., 2018). With the implementation of pollution mitigation strategies, the O_3 concentration was observed to be increased in the urban environment, which will lead to an increasing f_{NO2}, and therefore the corresponding $\delta^{15}N$–NO_3^- was expected to decline. Moreover, the changing fractional contribution of different oxidation pathways also cannot account for the consistent values of $\delta^{15}N$–NO_3^- in winter from 2013 to 2017, because the ^{15}N fractionation factors (εN) were comparable among the major oxidation pathways (Song et al., 2020). For example, the εN values for OH and N_2O_5 pathways in winter Beijing were predicted to be 33.0‰ and 30.7‰, respectively, while the whole εN value from NO*x* to NO_3^- was estimated to be 15.6‰ (Song et al., 2020). To elucidate the emission source effect, we simply assumed that the NO*x* emission from coal combustion in winter 2017 was entirely replaced by natural gas usage, while other sources remain stable. This would result in nearly 10‰ units ^{15}N-depleted in the NO_3^-, assuming the contribution of coal combustion accounted for approximately 30% (proportion was determined by Song et al., 2019a,b). This implied that other sources (e.g., vehicular exhaust or biomass burning) was tended to be ^{15}N-enriched or the emission strength of ^{15}N-enriched sources was enhanced during this period, which can counteract the effect of "Coal Replacing Project". To the best of our knowledge, NO*x* emitted from all the sectors was simulated to decline from 2013 to 2017, with the contribution of 47% of vehicle emission controls and 22.0% of coal-fired boiler controls for the overall NO*x* reduction in Beijing (Cheng et al., 2019). One of the measures to reduce vehicular NO*x* emission was the implementation of post-combustion catalytic NO*x* reduction technology (e.g., three-way catalytic converter), which was suggested to increase the $\delta^{15}N$-NO*x* values compared to NO*x* formed via combustion processes (Walters et al., 2015a, 2015b). Therefore, the gradually ^{15}N-enriched NO*x* emitted from the vehicle may be the primary driver that counteracted the effect of coal replacing project during the clean air action period. Taken together, one of the most possible explanations, as we noticed, was that the emission sources of NO*x* from 2013 to 2017 of winter Beijing were dominated by vehicle exhaust, rather than the coal or gas combustion. Correspondingly, using the measured $\delta^{15}N$–NO_3^- values, the εN values (15.6‰±7.4‰, Song et al., 2020), and the sources $\delta^{15}N$ signatures, the relative contribution of major NO*x* sources to NO_3^- in $PM_{2.5}$ were simulated using Bayesian mixing model of SIMMs (Zhang et al., 2020b). The model output indicated that the proportional contributions of vehicle exhaust and biomass burning were up to 70%, consistent with our speculation (Fig. S9). However, the Bayesian mixing model cannot distinguish the NO*x* from vehicle exhaust and biomass burning very well, due to the significant overlap of the $\delta^{15}N$ signatures of the two sources (see 2.5). Meanwhile, the proportional contribution of biomass burning may be overestimated since biomass burning related organic aerosol and black carbon was measured to decrease significantly (>50%) from 2014 to 2016 (Xu et al., 2019), as traditional biofuels represented by wood and crop residuals have been forbidden by the end of 2016. Concludingly, the results may suggest the predominant role of vehicle exhaust emission in the ambient NO*x*, consistent with the emission inventory approaches. For instance, Cheng et al., (2019) suggested that mobile sources dominated the NO*x* emission in Beijing in 2013, with a proportion of 67.2%. However, we must state that our speculation was controversial because that most of the $\delta^{15}N$ end-member values of major NO*x* sources in China have not been verified, although the few reports suggested the similarity of values or ranges compared with reports at other sites worldwide. Due to the overlap of ranges for vehicle exhaust and biomass burning, the source appointment of the two emission sources based on the Bayesian mixing model was usually biased. Therefore, the future study on the source $\delta^{15}N$ signatures of regional NO*x* is urgent.

4. Conclusion and remarks

Explosively growth of nitrate-dominate fine aerosol has been characterized as a major driver of haze pollution in recent years in urban cities of China. Therefore, a better constraining on the transformation dynamics of NO*x* to NO_3^- is helpful to better understand the haze formation mechanisms and further develop corresponding mitigation strategies. One of the advantages of the present study is the amelioration of the end-member $\delta^{18}O$ values generated by daytime and nocturnal pathways. We demonstrated that the Keeling plots ($\delta^{18}O$–NO_3^- against 1/NO_3^-) provided endmember values of $\delta^{18}O$– NO_3^- through the nocturnal pathway. The predicted $\delta^{18}O$ value for the ·OH oxidation pathway was 54.8‰, while for N_2O_5 hydrolysis pathway was approximately 95‰ for winter seasons in 2017. The isotopic mixing model also explicitly defined the proportional contribution of process-specific contributions to NO_3^- product, with a relatively narrow confidential interval (5%) compared with the commonly applied theoretical approach. In general, the NO_3^- from ·OH pathways contributed approximately 48% to the sink of NO_3^- of wintertime $PM_{2.5}$ in 2017. By comparing the determined $\delta^{15}N$–NO_3^- values (2017 *vs* 2013–2014) and the atmospheric conditions, we speculated that the major NO*x* emission sources included vehicle exhaust and biomass burning (>70%), which may be useful for mitigating atmospheric fine particle pollution in urban environments of Beijing.

The isotopic tracing approach is undoubtfully promising in the estimation of source contribution and chemical process of atmospheric nitrate pollutes. However, considerable uncertainties of isotopic signatures in several keystone molecules (e.g., $\delta^{15}N$ signatures of emitted NO*x*, end-member values of specific oxidation pathways, and $\delta^{18}O$ of water vapor) and parameters (e.g., f_{NO2}) would weak the significance of the overall estimation in mathematics and scientific senses, to a large extent. In addition, our approach cannot account for the relative importance of RO_2 chemistry in NO*x* cycling, which may result in some uncertainty in the following estimation of NO*x* conversion and specific source contribution. For the improvement of the isotopic tracing approach in tracking the source information of atmospheric NO*x*, we suggest that these abovementioned uncertainties should be better constrained or revealed in the future.

CRediT authorship contribution statement

Zhongyi Zhang: Conceptualization, Software, Investigation, Writing - original draft. **Hui Guan:** Conceptualization, Software, Investigation, Writing - original draft. **Li Luo:** Methodology, Resources, Writing -

review & editing, Data curation. **Nengjian Zheng:** Resources, Writing - review & editing, Data curation. **Hongwei Xiao:** Resources, Writing - review & editing, Supervision. **Yue Liang:** Resources, Writing - review & editing, Supervision. **Huayun Xiao:** Funding acquisition, Project administration, Supervision, Validation, Writing - review & editing.

Declaration of competing interest

The authors declare that they have no known competing financial interests or personal relationships that could have appeared to influence the work reported in this paper.

Acknowledgments

This study was kindly supported by the National Natural Science Foundation of China through grants 41863001, 41425014, and 41763001, Key Laboratory Project of Jiangxi Province (20171BCD40010) and Two 1000 Talents Plan Project of Jiangxi Province (S2018CQKJ0755). The data used in this manuscript is available in the supporting information or can be requested by contacting the principal investigator, Huayun Xiao (xiaohuayun@ecut.edu.cn).

Appendix A. Supplementary data

Supplementary data to this article can be found online at https://doi.org/10.1016/j.atmosenv.2020.117842.

References

Alexander, B., Hastings, M., Allman, D., Dachs, J., Thornton, J., Kunasek, S., 2009. Quantifying atmospheric nitrate formation pathways based on a global model of the oxygen isotopic composition ($\Delta^{17}O$) of atmospheric nitrate. Atmos. Chem. Phys. 9, 5043–5056.

An, Z., Huang, R.-J., Zhang, R., Tie, X., Li, G., Cao, J., Zhou, W., Shi, Z., Han, Y., Gu, Z., Ji, Y., 2019. Severe haze in northern China: a synergy of anthropogenic emissions and atmospheric processes. Proc. Natl. Acad. Sci. U.S.A. 116, 8657–8666.

Casciotti, K.L., Sigman, D.M., Hastings, M.G., Böhlke, J., Hilkert, A., 2002. Measurement of the oxygen isotopic composition of nitrate in seawater and freshwater using the denitrifier method. Anal. Chem. 74, 4905–4912.

Chang, Y., Ma, H., 2016. Comment on "Fossil fuel combustion-related emissions dominate atmospheric ammonia sources during severe haze episodes: evidence from ^{15}N-stable isotope in size-resolved aerosol ammonium". Environ. Sci. Technol. 50, 10765–10766.

Chang, Y., Zhang, Y.-L., Li, J., Tian, C., Song, L., Zhai, X., Zhang, W., Huang, T., Lin, Y.-C., Zhu, C., Fang, Y., Lehmann, M.F., Chen, J., 2019. Isotopic constraints on the atmospheric sources and formation of nitrogenous species in clouds influenced by biomass burning. Atmos. Chem. Phys. 19, 12221–12234.

Chen, Y., Wolke, R., Ran, L., Birmili, W., Spindler, G., Schröder, W., Su, H., Cheng, Y., Tegen, I., Wiedensohler, A., 2018. A parameterization of the heterogeneous hydrolysis of N_2O_5 for mass-based aerosol models: improvement of particulate nitrate prediction. Atmos. Chem. Phys. 18, 673–689.

Cheng, J., Su, J., Cui, T., Li, X., Dong, X., Sun, F., Yang, Y., Tong, D., Zheng, Y., Li, Y., 2019. Dominant role of emission reduction in $PM_{2.5}$ air quality improvement in Beijing during 2013–2017: a model-based decomposition analysis. Atmos. Chem. Phys. 19, 6125–6146.

Cohen, A.J., Brauer, M., Burnett, R., Anderson, H.R., Frostad, J., Estep, K., Balakrishnan, K., Brunekreef, B., Dandona, L., Dandona, R., 2017. Estimates and 25-year trends of the global burden of disease attributable to ambient air pollution: an analysis of data from the Global Burden of Diseases Study 2015. Lancet 389, 1907–1918.

Ding, J., Zhao, P., Su, J., Dong, Q., Du, X., Zhang, Y.J.A.C., 2019. Aerosol pH and its driving factors in Beijing. Atmos. Chem. Phys. 19, 7939–7954.

Elliott, E.M., Yu, Z., Cole, A.S., Coughlin, J.G., 2019. Isotopic advances in understanding reactive nitrogen deposition and atmospheric processing. Sci. Total. Environ. 662, 393–403.

Fang, Y.T., Koba, K., Wang, X.M., Wen, D.Z., Li, J., Takebayashi, Y., Liu, X.Y., Yoh, M., 2011. Anthropogenic imprints on nitrogen and oxygen isotopic composition of precipitation nitrate in a nitrogen-polluted city in southern China. Atmos. Chem. Phys. 11 (3), 1313.

Fang, Y.T., Koba, K., Makabe, A., Takahashi, C., Zhu, W., Hayashi, T., Hokari, A.A., Urakawa, R., Bai, E., Houlton, 2015. Microbial denitrification dominates nitrate losses from forest ecosystems. Proc. Natl. Acad. Sci. U.S.A. 112, 1470–1474.

Felix, J.D., Elliott, E.M., 2014. Isotopic composition of passively collected nitrogen dioxide emissions: vehicle, soil and livestock source signatures. Atmos. Environ. 92, 359–366.

Felix, J.D., Elliott, E.M., Shaw, S.L., 2012. Nitrogen isotopic composition of coal-fired power plant NOx: influence of emission controls and implications for global emission inventories. Environ. Sci. Technol. 46, 3528–3535.

Fountoukis, C., Nenes, A., 2007. ISORROPIA II: a computationally efficient thermodynamic equilibrium model for K^+–Ca^{2+}–Mg^{2+}–NH_4^+–Na^+–SO_4^{2-}–NO_3^-–Cl^-–H_2O aerosols. Atmos. Chem. Phys. 7, 4639–4659.

Gao, M., Liu, Z., Zheng, B., Ji, D., Sherman, P., Song, S., Xin, J., Liu, C., Wang, Y., Zhang, Q., 2019. China's Clean Air Action has suppressed unfavorable influences of climate on wintertime PM2. 5 concentrations in Beijing since 2002. Atmos. Chem. Phys. Discuss. 1–19.

Guo, H., Otjes, R., Schlag, P., Kiendler-Scharr, A., Nenes, A., Weber, R.J., 2018. Effectiveness of ammonia reduction on control of fine particle nitrate. Atmos. Chem. Phys. 18, 12241–12256.

Guo, H., Xu, L., Bougiatioti, A., Cerully, K.M., Capps, S.L., Hite, J.R., Carlton, A.G., Lee, S. H., Bergin, M.H., Ng, N.L., Nenes, A., Weber, R.J., 2015. Fine-particle water and pH in the southeastern United States. Atmos. Chem. Phys. 15, 5211–5228.

He, P., Xie, Z., Chi, X., Yu, X., Fan, S., Kang, H., Liu, C., Zhan, H., 2018. Atmospheric $\Delta^{17}O(NO_3^-)$ reveals nocturnal chemistry dominates nitrate production in Beijing haze. Atmos. Chem. Phys. 18, 14465–14476.

He, K., Zhang, Q., 2018. Trends in China's anthropogenic emissions since 2010 as the consequence of clean air actions. Atmos. Chem. Phys. 18, 14095–14111.

Li, H., Cheng, J., Zhang, Q., Zheng, B., Zhang, Y., Zheng, G., He, K., 2019. Rapid transition in winter aerosol composition in Beijing from 2014 to 2017: response to clean air actions. Atmos. Chem. Phys. 19, 11485–11499.

Li, H., Zhang, Q., Zheng, B., Chen, C., Wu, N., Guo, H., Zhang, Y., Zheng, Y., Li, X., He, K., 2018. Nitrate-driven urban haze pollution during summertime over the North China Plain. Atmos. Chem. Phys. 18, 5293–5306.

Liu, M., Song, Y., Zhou, T., Xu, Z., Yan, C., Zheng, M., Wu, Z., Hu, M., Wu, Y., Zhu, T., 2017. Fine particle pH during severe haze episodes in northern China. Geophys. Res. Lett. 44, 5213–5221.

Lu, K., Fuchs, H., Hofzumahaus, A., Tan, Z., Wang, H., Zhang, L., Schmitt, S.H., Rohrer, F., Bohn, B., Broch, S., 2019. Fast photochemistry in wintertime haze: consequences for pollution mitigation strategies. Environ. Sci. Technol. 53, 10676–10684.

Luo, L., Wu, Y., Xiao, H., Zhang, R., Lin, H., Zhang, X., Kao, S.-j., 2019. Origins of aerosol nitrate in Beijing during late winter through spring. Sci. Total. Environ. 653, 776–782.

Michalski, G., Bhattacharya, S., Mase, D.F., 2012. Oxygen Isotope Dynamics of Atmospheric Nitrate and its Precursor Molecules, Handbook of Environmental Isotope Geochemistry. Springer, pp. 613–635.

Mitroo, D., Gill, T.E., Haas, S., Pratt, K.A., Gaston, C., 2019. $ClNO_2$ production from N_2O_5 uptake on saline playa dusts: new insights into potential inland sources of $ClNO_2$. Environ. Sci. Technol. 53, 7442–7452.

Pataki, D., Ehleringer, J., Flanagan, L., Yakir, D., Bowling, D., Still, C., Buchmann, N., Kaplan, J., Berry, J., 2003. The application and interpretation of Keeling plots in terrestrial carbon cycle research. Global. Biogeochem. Cycles 17, 1022.

Phillips, D.L., Gregg, J.W., 2001. Uncertainty in source partitioning using stable isotopes. Oecologia 127, 171–179.

Shah, V., Jaeglé, L., Thornton, J.A., Lopez-Hilfiker, F.D., Lee, B.H., Schroder, J.C., Campuzano-Jost, P., Jimenez, J.L., Guo, H., Sullivan, A.P., Weber, R.J., Green, J.R., Fiddler, M.N., Bililign, S., Campos, T.L., Stell, M., Weinheimer, A.J., Montzka, D.D., Brown, S.S., 2018. Chemical feedbacks weaken the wintertime response of particulate sulfate and nitrate to emissions reductions over the eastern United States. Proc. Natl. Acad. Sci. U.S.A. 115, 8110–8115.

Shi, X., Nenes, A., Xiao, Z., Song, S., Yu, H., Shi, G., Zhao, Q., Chen, K., Feng, Y., Russell, A.G., 2019. High-resolution data sets unravel the effects of sources and meteorological conditions on nitrate and its gas-particle partitioning. Environ. Sci. Technol. 53, 3048–3057.

Sigman, D.M., Casciotti, K.L., Andreani, M., Barford, C., Galanter, M., Böhlke, J., 2001. A bacterial method for the nitrogen isotopic analysis of nitrate in seawater and freshwater. Anal. Chem. 73, 4145–4153.

Song, W., Liu, X.-Y., Wang, Y.-L., Tong, Y.-D., Bai, Z.-P., Liu, C.-Q., 2020. Nitrogen isotope differences between atmospheric nitrate and corresponding nitrogen oxides: a new constraint using oxygen isotopes. Sci. Total Environ. 701, 134515.

Song, S., Nenes, A., Gao, M., Zhang, Y., Liu, P., Shao, J., Ye, D., Xu, W., Lei, L., Sun, Y., 2019a. Thermodynamic modeling suggests declines in water uptake and acidity of inorganic aerosols in Beijing winter haze events during 2014/2015–2018/2019. Environ. Sci. Technol. Lett. 6 (12), 752–760.

Song, W., Wang, Y.-L., Yang, W., Sun, X.-C., Tong, Y.-D., Wang, X.-M., Liu, C.-Q., Bai, Z.-P., Liu, X.-Y., 2019b. Isotopic evaluation on relative contributions of major NOx sources to nitrate of $PM_{2.5}$ in Beijing. Environ. Pollut. 248, 183–190.

Sun, Y., Chen, C., Zhang, Y., Xu, W., Zhou, L., Cheng, X., Zheng, H., Ji, D., Li, J., Tang, X., 2016. Rapid formation and evolution of an extreme haze episode in Northern China during winter 2015. Sci. Rep. 6, 27151.

Tan, Zhaofeng, Rohrer, Franz, Lu, Keding, Ma, Xuefei, Bohn, Birger, Broch, Briger, Dong, Huabin, Fuchs, Hendrik, Gkatzeils, Georgios I., Hofzumahaus, Andreas, Holland, Frank, Li, Xin, Liu, Ying, Liu, Yuhan, Novelli, Anna, Shao, Min, Wang, Haichao, Wu, Yusheng, Zeng, Limin, Hu, Min, Zhang, Yuanhang, et al., 2018. Wintertime photochemistry in Beijing: observations of ROx radical concentrations in the North China Plain during the BEST-ONE campaign. Atmos. Chem. Phys. 18 (16), 12391–12411.

Tian, M., Liu, Y., Yang, F., Zhang, L., Peng, C., Chen, Y., Shi, G., Wang, H., Luo, B., Jiang, C., Li, B., Takeda, N., Koizumi, K., 2019. Increasing importance of nitrate formation for heavy aerosol pollution in two megacities in Sichuan Basin, southwest China. Environ. Pollut. 250, 898–905.

Walters, W.W., Fang, H., Michalski, G., 2018. Summertime diurnal variations in the isotopic composition of atmospheric nitrogen dioxide at a small midwestern United States city. Atmos. Environ. 179, 1–11.
Walters, W.W., Goodwin, S.R., Michalski, G., 2015a. Nitrogen stable isotope composition ($\delta^{15}N$) of vehicle-emitted NO*x*. Environ. Sci. Technol. 49, 2278–2285.
Walters, W.W., Michalski, G., 2015. Theoretical calculation of nitrogen isotope equilibrium exchange fractionation factors for various NOy molecules. Geochem. Cosmochim. Acta 164, 284–297.
Walters, W.W., Michalski, G., 2016. Theoretical calculation of oxygen equilibrium isotope fractionation factors involving various NO molecules, OH, and H_2O and its implications for isotope variations in atmospheric nitrate. Geochem. Cosmochim. Acta 191, 89–101.
Walters, W.W., Simonini, D.S., Michalski, G., 2016. Nitrogen isotope exchange between NO and NO_2 and its implications for $\delta^{15}N$ variations in tropospheric NOx and atmospheric nitrate. Geophys. Res. Lett. 43, 440–448.
Walters, W.W., Tharp, B.D., Fang, H., Kozak, B.J., Michalski, G., 2015b. Nitrogen isotope composition of thermally produced NO*x* from various fossil-fuel combustion sources. Environ. Sci. Technol. 49, 11363–11371.
Wang, H., Lu, K., Chen, X., Zhu, Q., Chen, Q., Guo, S., Jiang, M., Li, X., Shang, D., Tan, Z., 2017a. High N_2O_5 concentrations observed in urban Beijing: implications of a large nitrate formation pathway. Environ. Sci. Technol. Lett. 4, 416–420.
Wang, H., Lu, K., Chen, X., Zhu, Q., Wu, Z., Wu, Y., Sun, K., 2018. Fast particulate nitrate formation via N_2O_5 uptake aloft in winter in Beijing. Atmos. Chem. Phys. 18, 10483–10495.
Wang, X., Wang, H., Xue, L., Wang, T., Wang, L., Gu, R., Wang, W., Tham, Y.J., Wang, Z., Yang, L., 2017b. Observations of N_2O_5 and $ClNO_2$ at a polluted urban surface site in North China: high N2O5 uptake coefficients and low ClNO2 product yields. Atmos. Environ. 156, 125–134.
Wang, Y., Li, W., Gao, W., Liu, Z., Tian, S., Shen, R., Ji, D., Wang, S., Wang, L., Tang, G., 2019a. Trends in particulate matter and its chemical compositions in China from 2013–2017. Sci. China-Earth Sci. 1–15.
Wang, Y.L., Song, W., Yang, W., Sun, X.C., Tong, Y.D., Wang, X.M., Liu, C.Q., Bai, Z.P., Liu, X.Y., 2019b. Influences of atmospheric pollution on the contributions of major oxidation pathways to $PM_{2.5}$ nitrate formation in Beijing. J. Geophys. Res. Atmos. 124, 4174–4185.
Wen, L., Chen, J., Yang, L., Wang, X., Xu, C., Sui, X., Yao, L., Zhu, Y., Zhang, J., Zhu, T., 2015. Enhanced formation of fine particulate nitrate at a rural site on the North China Plain in summer: the important roles of ammonia and ozone. Atmos. Environ. 101, 294–302.
Wen, L., Xue, L., Wang, X., Xu, C., Chen, T., Yang, L., Wang, T., Zhang, Q., Wang, W., 2018. Summertime fine particulate nitrate pollution in the North China Plain: increasing trends, formation mechanisms and implications for control policy. Atmos. Chem. Phys. 18, 11261–11275.
Xiao, H.-W., Xie, L.-H., Long, A.-M., Ye, F., Pan, Y.-P., Li, D.-N., Long, Z.-H., Chen, L., Xiao, H.-Y., Liu, C.-Q., 2015. Use of isotopic compositions of nitrate in TSP to identify sources and chemistry in South China Sea. Atmos. Environ. 109, 70–78.
Xie, Y., Wang, G., Wang, X., Chen, J., Chen, Y., Tang, G., Wang, L., Ge, S., Xue, G., Wang, Y., Gao, J., 2019. Observation of nitrate dominant PM2.5 and particle pH elevation in urban Beijing during the winter of 2017. Atmos. Chem. Phys. Discuss. 1–25, 2019.
Xu, W., Sun, Y., Wang, Q., Zhao, J., Wang, J., Ge, X., Xie, C., Zhou, W., Du, W., Li, J., Fu, P., Wang, Z., Worsnop, D.R., Coe, H., 2019. Changes in aerosol chemistry from 2014 to 2016 in winter in Beijing: insights from high-resolution aerosol mass spectrometry. J. Geophys. Res. Atmos. 124, 1132–1147.
Yan, C., Tham, Y.J., Zha, Q., Wang, X., Xue, L., Dai, J., Wang, Z., Wang, T., 2019. Fast heterogeneous loss of N_2O_5 leads to significant nighttime NOx removal and nitrate aerosol formation at a coastal background environment of southern China. Sci. Total Environ. 677, 637–647.
Yang, J.-Y., Hsu, S.-C., Dai, M., Hsiao, S.-Y., Kao, S.-J., 2014. Isotopic composition of water-soluble nitrate in bulk atmospheric deposition at Dongsha Island: sources and implications of external N supply to the northern South China Sea. Biogeosciences 11, 1833.
Yun, H., Wang, W., Wang, T., Xia, M., Yu, C., Wang, Z., Poon, S.C.N., Yue, D., Zhou, Y., 2018. Nitrate formation from heterogeneous uptake of dinitrogen pentoxide during a severe winter haze in southern China. Atmos. Chem. Phys. 18, 17515–17527.
Zhang, Q., Zheng, Y., Tong, D., Shao, M., Wang, S., Zhang, Y., Xu, X., Wang, J., He, H., Liu, W., Ding, Y., Lei, Y., Li, J., Wang, Z., Zhang, X., Wang, Y., Cheng, J., Liu, Y., Shi, Q., Yan, L., Geng, G., Hong, C., Li, M., Liu, F., Zheng, B., Cao, J., Ding, A., Gao, J., Fu, Q., Huo, J., Liu, B., Liu, Z., Yang, F., He, K., Hao, J., 2019. Drivers of improved $PM_{2.5}$ air quality in China from 2013 to 2017. Proc. Natl. Acad. Sci. U.S.A. 116 (49), 24463–24469.
Zhang, Z., Zeng, Y., Zheng, N., Luo, L., Xiao, H., Xiao, H., 2020a. Fossil fuel-related emissions were the major source of NH_3 pollution in urban cities of northern China in the autumn of 2017. Environ. Pollut. 256, 113428.
Zhang, Z., Zheng, N., Zhang, D., Xiao, H., Cao, Y., Xiao, H., 2020b. Rayleigh based concept to track NOx emission sources in urban areas of China. Sci. Total Environ. 704, 135362, 2020b.
Zheng, B., Tong, D., Li, M., Liu, F., Hong, C., Geng, G., Li, H., Li, X., Peng, L., Qi, J., Yan, L., Zhang, Y., Zhao, H., Zheng, Y., Zheng, B., Zhang, Q., Zhang, Y., He, K., Wang, K., Zheng, G., Duan, F., Ma, Y., Kimoto, T., 2015. Heterogeneous chemistry: a mechanism missing in current models to explain secondary inorganic aerosol formation during the January 2013 haze episode in North China. Atmos. Chem. Phys. 15.
Zhou, W., Gao, M., He, Y., Wang, Q., Xie, C., Xu, W., Zhao, J., Du, W., Qiu, Y., Lei, L., Fu, P., Wang, Z., Worsnop, D.R., Zhang, Q., Sun, Y., 2019. Response of aerosol chemistry to clean air action in Beijing, China: insights from two-year ACSM measurements and model simulations. Environ. Pollut. 255, 113345.
Zong, Z., Wang, X., Tian, C., Chen, Y., Fang, Y., Zhang, F., Li, C., Sun, J., Li, J., Zhang, G., 2017. First assessment of NOx sources at a regional background site in north China using isotopic analysis linked with modeling. Environ. Sci. Technol. 51, 5923–5931.